Monthly Notices of the ROYAL ASTRONOMICAL SOCIETY

MNRAS **467,** 1202–1208 (2017) doi:10.1093/mnras/stx141
Advance Access publication 2017 January 18

Optically thick envelopes around ULXs powered by accreating neutron stars

Alexander A. Mushtukov,[1,2,3]★ Valery F. Suleimanov,[4] Sergey S. Tsygankov[5] and Adam Ingram[1]

[1]*Anton Pannekoek Institute, University of Amsterdam, Science Park 904, NL-1098 XH Amsterdam, the Netherlands*
[2]*Space Research Institute of the Russian Academy of Sciences, Profsoyuznaya Str 84/32, Moscow 117997, Russia*
[3]*Pulkovo Observatory, Russian Academy of Sciences, Saint Petersburg 196140, Russia*
[4]*Institut für Astronomie und Astrophysik, Universität Tübingen, Sand 1, D-72076 Tübingen, Germany*
[5]*Tuorla observatory, Department of Physics and Astronomy, University of Turku, Väisäläntie 20, FI-21500 Piikkiö, Finland*

Accepted 2017 January 13. Received 2017 January 13; in original form 2016 December 3

ABSTRACT

Magnetized neutron stars power at least some ultraluminous X-ray sources. The accretion flow in these cases is interrupted at the magnetospheric radius and then reaches the surface of a neutron star following magnetic field lines. Accreting matter moving along magnetic field lines forms the accretion envelope around the central object. We show that in case of high-mass accretion rates $\gtrsim 10^{19}$ g s^{-1} the envelope becomes closed and optically thick, which influences the dynamics of the accretion flow and the observational manifestation of the neutron star hidden behind the envelope. Particularly, the optically thick accretion envelope results in a multi-colour blackbody spectrum originating from the magnetospheric surface. The spectrum and photon energy flux vary with the viewing angle, which gives rise to pulsations characterized by high pulsed fraction and typically smooth pulse profiles. The reprocessing of radiation due to interaction with the envelope leads to the disappearance of cyclotron scattering features from the spectrum. We speculate that the super-orbital variability of ultraluminous X-ray sources powered by accreting neutron stars can be attributed to precession of the neutron star due to interaction of magnetic dipole with the accretion disc.

Key words: magnetic fields – radiative transfer – scattering – stars: neutron – X-rays: binaries.

1 INTRODUCTION

Accretion on to a highly magnetized (surface magnetic field $B \gtrsim 10^{12}$ G) neutron star (NS) is governed by the magnetic field of the central object. Namely, the accretion disc is interrupted at the magnetospheric radius $R_{\rm m}$, where the magnetic pressure becomes comparable to ram pressure (due to Keplerian motion) of accreting material. Then the matter (a) follows magnetic field lines, (b) is accumulated at the magnetosphere (Siuniaev & Shakura 1977) or (c) is pushed away from the system depending on magnetic field strength, mass accretion rate and NS spin period (Shtykovskiy & Gilfanov 2005; Tsygankov et al. 2016a). If the matter continues its movement along magnetic field lines, it reaches the NS surface at small regions in the vicinity of the magnetic poles. There the matter releases its kinetic energy mostly in X-rays. This gives rise to X-ray pulsar (XRP) phenomenon (see Walter et al. 2015 for recent review). The mass accretion rate, surface magnetic field structure and strength affect the geometry of the illuminating region (Basko & Sunyaev 1976b; Mushtukov et al. 2015b). Accretion luminosity of XRPs can be close or even higher than the Eddington luminosity. Recent discoveries of pulsating ultraluminous X-ray sources (ULXs) show that XRP accretion luminosity can be as high as 10^{40}–10^{41} erg s^{-1}, which is a few hundreds times higher than the Eddington value for an NS (Bachetti 2014; Israel 2016b, 2017; Fürst et al. 2016).

ULXs powered by accreting NSs require special geometrical and physical conditions at the emitting region. It is known that a high-mass accretion rate leads to the appearance of an accretion column above the surface of the NS (Basko & Sunyaev 1976b; Mushtukov et al. 2015b). The accretion flow is stopped at the top of the column in a radiation-dominated shock and then slowly settles down to the surface. The column can be as high as the NS radius (Poutanen et al. 2013) and the material is confined there by magnetic field. It explains how accretion luminosity can principally exceed the Eddington limit (Mushtukov

★ E-mail: al.mushtukov@gmail.com

et al. 2015a). It is also important that the effective scattering cross-section and, therefore, radiation pressure are reduced by strong magnetic field (Harding & Lai 2006; Mushtukov, Nagirner & Poutanen 2012, 2016).

There are still debates on the magnetic field strength in recently discovered ULXs powered by magnetized NSs. The model of beamed X-ray sources fed at a super-Eddington accretion rate infers relatively weak magnetic field $\sim 10^{11}$ G (King & Lasota 2016). Assuming torque equilibrium and solving the torque equation instead leads to B-field strength of $(2\div 7)\times 10^{13}$ G (Ekşi et al. 2015) or lower $\sim 10^{13}$ G (Dall'Osso, Perna & Stella 2015) depending on model assumptions, which are essential near the equilibrium (Parfrey, Spitkovsky & Beloborodov 2016). Transitions of ULX M82 X-2 between high and low states were interpreted as a 'propeller effect, requiring magnetar-like magnetic field $\sim 10^{14}$ G (Tsygankov et al. 2016b). This is in good agreement with predictions of a model of accretion column (Mushtukov et al. 2015a).

The dynamics of the flow in the accretion envelope (curtain) were assumed to be unaffected by radiation pressure so far. However, this is not the case for ULXs powered by accreting NSs. In this case, the accretion flow between the inner disc radius and NS surface should be affected by radiation pressure. Moreover, simple estimations show that the accretion curtain at accretion luminosity $L \gtrsim 10^{40}$ erg s^{-1} becomes optically thick and shields the central object completely. It should influence the observational manifestation of bright XRPs. The possibility of NS shielding of by optically thick medium was supposed earlier (Ekşi et al. 2015) in order to explain null result of search of pulsations in archival *XMM–Newton* observations of several ULXs performed by Doroshenko, Santangelo & Ducci (2015).

In this paper, we discuss properties of accretion curtain at the magnetosphere of ultraluminous XRPs. We pay attention to its observational manifestation in spectral and timing properties of ULXs.

2 BASIC IDEAS

2.1 Accretion flow at the magnetospheric surface

The accretion disc is interrupted at the magnetospheric radius (Lai 2014), given by

$$R_{\rm m} = 7\times 10^7 \Lambda\, m^{1/7} R_6^{10/7} B_{12}^{4/7} L_{39}^{-2/7}\ {\rm cm}, \quad (1)$$

where $m = {\rm M}/{\rm M}_\odot$ is NS mass in units of solar masses, $B_{12} = B/10^{12}$ G is surface magnetic field strength, $L_{39} = L/10^{39}$ erg s^{-1} is the accretion luminosity, $R_6 = R/10^6$ cm is the NS radius and Λ is a constant that depends on the accretion flow geometry with $\Lambda = 0.5$ being a commonly used value for the case of disc accretion. From the magnetospheric radius, the matter follows dipole magnetic field lines (Frank, King & Raine 2002), which are described by the relation

$$r(\lambda) = R_{\rm m}\cos^2\lambda, \quad (2)$$

where λ is the angular coordinate measured from the accretion disc plane and $r(\lambda)$ is a distance from the central object to a given point at the magnetic dipole line (see Fig. 1).

The optical thickness of the flow at the magnetospheric surface is defined by the mass accretion rate $\dot{M}$, local velocity $v(\lambda)$ and mechanism of opacity. For the case of ionized gas at temperature $T > 10^7$ K, the opacity is defined by electron scattering (at lower temperature the Kramer opacity dominates with much higher cross-sections and optical thickness) and local optical thickness is

$$\tau_{\rm e}(\lambda) \approx \frac{\kappa_{\rm e}\dot{M} d_0}{2 S_{\rm D} v(\lambda)}\left(\frac{\cos\lambda_0}{\cos\lambda}\right)^3 \approx \frac{70\, L_{39}^{6/7} B_{12}^{2/7}}{\beta(\lambda)}\left(\frac{\cos\lambda_0}{\cos\lambda}\right)^3, \quad (3)$$

where $\beta(\lambda) = v(\lambda)/c$ is local dimensionless velocity along magnetic field lines, $S_{\rm D} \sim 10^{10}$ cm^2 is the area of accretion channel base at the NS surface, d_0 is the geometrical thickness of the channel at the base, $\lambda_0 \simeq \pi - (R/R_{\rm m})^{1/2}$ is the coordinate corresponding to the accretion channel base and $\kappa_{\rm e} = 0.34$ cm^2 g^{-1} is the Thomson electron scattering opacity for solar abundances.

The matter on the B-field lines moves under the influence of gravitational $\overline{f}_{\rm grav}$ and radiation $\overline{f}_{\rm rad}$ forces. If the photon flux is directed from the central object, the directions of the forces are opposite to each other. If the local magnetic field strength is sufficiently high and is not significantly disturbed by radiative force, the dynamics of the material at the field lines is defined by the longitudinal component of the resulting force. The angle between the radius-vector pointed to a given point at the dipole field line and the tangent to the field line (see Fig. 1) is

$$\chi = \arctan(0.5/\tan(\lambda)).$$

In the case of a rotating NS there is also a centrifugal force $\overline{f}_{\rm cent}$ in the corotating reference frame, which affects the dynamics of matter. The centrifugal force is directed perpendicular to the spin axis of an NS. Hence, the angle between the tangent to the field line and the centrifugal force is

$$\xi = \pi + \chi - \lambda.$$

The resulting force gives an acceleration along magnetic field lines $a_{||}(\lambda)$ and the velocity of accretion flow is described by

$$\beta\frac{{\rm d}\beta}{{\rm d}\lambda} = \frac{R_{\rm m}\cos\lambda(4-3\cos^2\lambda)^{1/2}}{c^2} a_{||}(\lambda), \quad (4)$$

where $a_{||}(\lambda)$ is acceleration along the magnetic field lines caused by the resulting force. This differential equation can be solved for known acceleration along magnetic field lines, given an initial velocity of material, mass accretion rate, surface magnetic field strength and spin period of the NS.

2.2 Closed optically thick magnetospheric envelopes

In the case of extremely high mass accretion rate $\dot{M} \gtrsim 2.5\times 10^{18}\Lambda^{21/22} B_{12}^{6/11} m^{-5/11}$, which corresponds to accretion luminosity

$$L \gtrsim 3.4\times 10^{38}\,\Lambda^{21/22} B_{12}^{6/11} m^{6/11}\ {\rm erg\ s^{-1}}, \quad (5)$$

the accretion disc becomes radiation dominated and geometrically thick (Shakura & Sunyaev 1973; Suleimanov, Lipunova & Shakura 2007). In this case, the accretion curtain is closed and radiation from the central object cannot leave freely the magnetosphere. Because the velocity along B-field lines cannot exceed the free-fall velocity, the optical thickness of the accretion curtain due to electron scattering $\tau_{\rm e}(\lambda) > \tau_{\rm e}(0) = L_{39}^{8/7} B_{12}^{-2/7}$ according to (3). Hence, the accretion curtain is optically thick if $L_{39} \gtrsim B_{12}^{1/4}$. At luminosity,

$$L \gtrsim 5.7\times 10^{39}\,\Lambda^{7/9} B_{12}^{4/9} m^{8/9} R_6^{1/3}\ {\rm erg\ s^{-1}} \quad (6)$$

accretion disc thickness at the magnetospheric radius $R_{\rm m}$ is comparable to the size of NS magnetosphere (Lipunov 1982).

The photons from the central object are more likely reprocessed and reflected back into the cavity formed by the dipole magnetosphere than to immediately penetrate through the envelope. Each

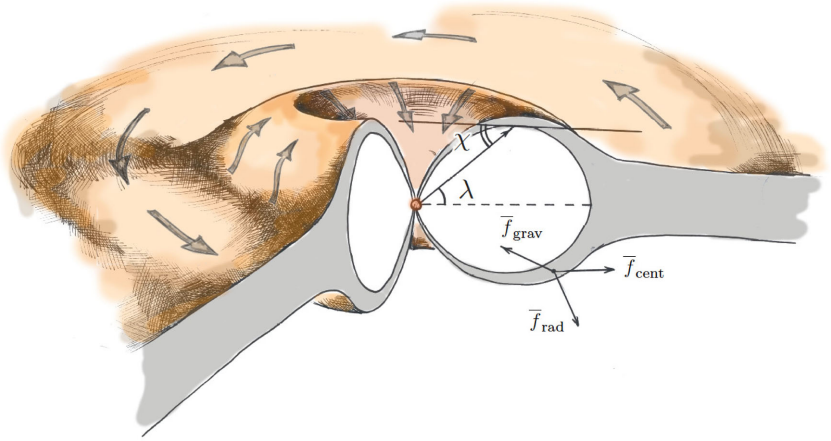

Figure 1. The structure of accretion flow in ULX powered by accreting NS. The geometrically thick accretion disc is interrupted at the magnetospheric radius and the accretion flow forms optically thick envelope. The inner part of dipolar magnetosphere is filled with hot thermolized photons. The observer detects the photons originated from the outer surface of magnetosphere.

photon undergoes a number of scattering before it leaves the system. Hence, the radiation field is in equilibrium inside the magnetosphere and can be roughly described by blackbody radiation of certain temperature $T_{\rm in}$, which is determined by the total accretion luminosity, the size of magnetosphere and its optical thickness.

Let us consider a simplified problem of a point source of luminosity $L_{\rm ps}$ surrounded by spherical envelope of radius $R_{\rm sp}$ and optical thickness $\tau_{\rm sp} \gg 1$. Then the outer temperature of the spherical envelope is related to the inner temperature $T_{\rm in}$ as $T_{\rm out} \approx T_{\rm in}\tau_{\rm sp}^{-1/4}$. Because the total luminosity is conserved, the outer temperature is related to the luminosity and geometrical size of the envelope: $\sigma_{\rm SB}T_{\rm out}^4 = L_{\rm ps}/(4\pi R_{\rm sp}^2)$. Then the internal temperature is $T_{\rm in} = [\tau_{\rm sp}L_{\rm ps}/(4\pi\sigma_{\rm SB}R_{\rm sp}^2)]^{1/4}$. In the case of a central source surrounded by a dipole surface, the internal temperature depends on the distribution of optical thickness over the surface.

The radiation force due to blackbody radiation in the magnetospheric cavity is directed perpendicularly to the magnetic field lines. As a result, the dynamics of the accretion flow along B-field lines is determined by gravity and centrifugal force only and described by the equation

$$\beta\frac{{\rm d}\beta}{{\rm d}\lambda} = \frac{GM(4-3\cos^2\lambda)^{1/2}}{c^2R_{\rm m}\cos^3\lambda} \times\left[\cos\chi + \left(\frac{\omega}{\omega_{\rm K}^*}\right)^2\cos^7\lambda\cos\xi\right]. \quad (7)$$

Despite high optical thickness of the accretion curtain, the photons penetrate through it after a number of scatterings. The time of photon diffusion through the accretion curtain is defined by local optical and geometrical thickness:

$$t_{\rm diff} \approx \frac{\tau(\lambda)d(\lambda)}{c} \sim 2\times10^{-9}\frac{L_{39}^{6/7}B_{12}^{2/7}d(\lambda)}{\beta(\lambda)}\left(\frac{\cos\lambda_0}{\cos\lambda}\right)^3 {\rm s}. \quad (8)$$

If the photon diffusion time is much smaller than the dynamical time-scale, the local flux at the outer side of a curtain is defined by the internal temperature and local optical thickness (Ivanov 1969):

$$T_{\rm out}(\lambda) \simeq T_{\rm in}\tau^{-1/4}(\lambda). \quad (9)$$

Because the temperature at the outer side of the curtain varies depending on the optical thickness, the whole accretion curtain radiates multi-colour blackbody radiation. The typical outer temperature can be roughly estimated as

$$T_{\rm out} \sim \left(\frac{L}{\sigma_{\rm SB}4\pi R_{\rm m}^2}\right)^{1/4} \approx 0.5\,L_{39}^{11/28}B_{12}^{-2/7}m^{-1/14}R_6^{-5/7}\ {\rm keV}. \quad (10)$$

The internal temperature is higher and has to be found numerically. We see that the temperature in the envelope is $\gtrsim 1$ keV for typical ULX luminosity and the opacity is, indeed, dominated by electron scattering.

The observed spectrum depends on the viewing angle as well because the observer sees different parts of the accretion curtain from different directions. The photon energy flux distribution over photon energy E is defined by the temperature distribution over the visible parts of the envelope and given by

$$F_E = \frac{2E^3}{h^3c^2}\frac{R_{\rm m}^2}{D^2}\int{\rm d}\varphi\int{\rm d}\lambda\cos i(\varphi,\theta)\frac{\cos^4\lambda(4-3\cos^2\lambda)^{1/2}}{\exp\left[\frac{E}{kT_{\rm out}(\lambda)}\right]-1},$$

where the integrals are taken over the visible part of magnetic dipole surface, i denotes the angle between the line of sight and local normal to the dipole surface and D is the distance from the NS to observer. If the typical time of photon diffusion through the accretion curtain (equation 8) is comparable to the dynamical time-scale (which can be the case at high luminosity $\gtrsim few\times 10^{40}$ erg s^{-1}), the final spectrum is disturbed.

The total luminosity of the accretion curtain can be obtained by integration of the flux over the dipole surface:

$$L = \frac{4\pi}{h^3c^2}R_{\rm m}^2\int_0^\infty{\rm d}E\,E^3\int_{\lambda_1}^{\lambda_2}{\rm d}\lambda\frac{\cos^4\lambda(4-3\cos^2\lambda)^{1/2}}{\exp\left[\frac{E}{kT_{\rm out}(\lambda)}\right]-1} \simeq 6.3\times10^{39}R_{\rm m,8}^2 \times\int_0^\infty{\rm d}E_{\rm keV}E_{\rm keV}^3\int_{\lambda_1}^{\lambda_2}{\rm d}\lambda\frac{\cos^4\lambda(4-3\cos^2\lambda)^{1/2}}{\exp\left[\frac{E}{kT_{\rm out}(\lambda)}\right]-1}$$

where $R_{\rm m,\,8} = R_{\rm m}/10^8$ cm and $E_{\rm keV} = E/1$ keV.

It has to be noted that accretion from the disc likely results in an accretion channel, where the matter is confined to a narrow wall of magnetic funnel. In this case, part of accretion column radiation can

be radiated into the outer part of the magnetospheric cavity. This part of radiation is not reprocessed by the optically thick accretion curtain and is represented by a power-law spectrum.

The accretion disc by itself can contribute to the X-ray flux at extreme mass accretion rates. The effective temperature of the disc at the magnetospheric radius $R_{\rm m}$ (equation 1) can be roughly estimated as

$$T_{\rm disc} \simeq 0.25\, L_{39}^{13/28} B_{12}^{-3/7} m^{-3/28} R_6^{-23/28}\ \text{keV}, \quad (11)$$

which is close to the temperature expected from the accretion envelope (equation 10). The energy spectrum of the accretion disc is likely given by milti-colour blackbody (Shakura & Sunyaev 1973), but can be disturbed due to advection. As a result, one can expect an additional non-pulsating component in spectrum of ULXs powered by accreting NSs.

The magnetic field strength at the magnetospheric surface should be high enough to confine the accretion flow affected by internal radiation pressure $P_{\rm rad} \approx aT_{\rm in}^4/3$. Then, the magnetic pressure

$$P_{\rm mag}(\lambda) = \frac{B^2(\lambda)}{8\pi}$$

should exceed $P_{\rm rad}$: $P_{\rm rad}/P_{\rm mag} \lesssim 1$. The magnetic field pressure can be estimated from below by

$$P_{\rm mag}(\lambda = 0) \simeq 3.4 \times 10^{11} \Lambda^{-6} B_{12}^{-10/7} L_{39}^{12/7} m^{-6/7} R_6^{-18/7}.$$

Using estimation of the outer temperature (equation 10) we get

$$\frac{P_{\rm rad}}{P_{\rm mag}} \lesssim 7 \times 10^{-2} \tau L_{39}^{-1/7} B_{12}^{2/7} m^{2/7} R_6^{-2/7}, \quad (12)$$

which turns to $P_{\rm rad}/P_{\rm mag} \lesssim 0.07\, L_{39} m^{2/7} R_6^{-2/7}$ in the case of accretion flow of free-fall velocity. Therefore, the accretion envelope can be unstable at accretion luminosity above 10^{40} erg s^{-1}, but this is beyond the scope of this work.

2.3 Interaction of the accretion curtain with X-ray photons in normal XRPs

XRPs usually show hard energy spectra well fitted by a broken power law and complicated pulse profiles (see Walter et al. 2015 for recent review). Accreting NSs in normal XRPs are surrounded by an accretion curtain of intermediate optical thickness and relatively low temperature. The principal mechanisms of interaction between photons and accretion curtain are photoionization of heavy elements and Compton scattering with the energy recoil effect when the photon energy $E \gg kT_{\rm e}$ (Syunyaev 1976). The photons originating from the emitting region (hot spots or accretion column) are reprocessed partially. The photons experience $\sim\tau_{\rm e}^2$ scattering on the average, where $\tau_{\rm e}$ is the optical thickness (Ivanov 1969; Illarionov & Syunyaev 1972). The initial energy of photons will be reduced due to the recoil effect from $E \gg kT_{\rm e}$ to $\sim \max(3k_{\rm B}T_{\rm e}, m_{\rm e}c^2/\tau_{\rm e}^2)$, which leads to effective energy absorption by the accretion curtain (Syunyaev 1976). The absorbed energy is re-emitted in the soft X-ray energy band. Because the plasma layer occupies only some part of the magnetospheric surface, it affects X-ray pulsations and can cause the complicated structure of pulse profiles (Basko & Sunyaev 1976a). A detailed discussion of effects arising from accretion curtain in normal XRPs is beyond the scope of this paper.

2.4 Power spectra affected by closed envelope

XRPs commonly show fast aperiodic variability of X-ray flux over a broad frequency range (similar variability is shown by accreting black holes, see Ingram 2016). The variability is explained by the propagating fluctuations model (Lyubarskii 1997). The initial mass accretion rate variability is produced all over accretion disc due to MHD processes (Balbus & Hawley 1991) and results in mass accretion rate variability at the magnetospheric radius (Lyubarskii 1997). In the case of normal XRPs, the observer detects photons directly from the emitting regions near the NS surface and variability of the mass accretion rate is directly imprinted in variability of observed X-ray flux (Revnivtsev et al. 2009), which provides the possibility of diagnostics of accretion disc. In case of extremely high mass accretion rate typical for ULXs, the optically thick envelope screens the direct X-ray flux originating from the vicinity of the NS and reprocesses it. Observed variability is defined by variability of the mass accretion rate at the NS surface and variability of the local mass accretion rate and optical thickness at the magnetospheric envelope. As a result, aperiodic variability of ULXs is expected to be suppressed on time-scales shorter than the time-scale of matter travel from the disc to the NS surface.

3 MODEL SET-UP

For simplicity and in order to get qualitative results, we consider the accretion disc to be aligned with the equatorial plane of magnetic dipole. Inclining the magnetic dipole field changes the equations, but the main physical ideas remain the same.

We consider a Keplerian accretion disc, where the angular velocity is given by

$$\Omega_{\rm K} = \left(\frac{GM}{R^3}\right)^{1/2} = 11.5 \left(\frac{m}{R_8^3}\right)^{1/2}\ \text{rad s}^{-1}. \quad (13)$$

The angular velocity of the magnetosphere is $\Omega = 2\pi/P$. If the mass accretion rate and accretion luminosity are higher than the limiting values corresponding to 'propeller' effect (see, e.g. Tsygankov et al. 2016a):

$$L_{\rm lim} \simeq 5 \times 10^{37} \Lambda^{7/2} B_{12}^2 P^{-7/3} m^{-2/7} R_6^5\ \text{erg s}^{-1}, \quad (14)$$

then the magnetospheric radius is smaller than the corotational radius and Keplerian angular velocity is higher than the angular velocity of NS magnetosphere. The accreting material looses its kinetic energy due to interaction with the magnetosphere. The lost energy is going into heat. The released energy is defined by the difference between Keplerian and magnetospheric angular velocities: $W_{\rm th} \propto (\Omega_{\rm K} - \Omega)^2$. The temperature caused by dissipation of kinetic energy is

$$T = \frac{1}{2}(\gamma - 1) T_{\rm vir} \left[1 - \frac{\Omega}{\Omega_{\rm K}}\right]^2, \quad (15)$$

where γ is the adiabatic index and the virial temperature is defined as

$$T_{\rm vir} = \frac{GM\mu}{R\mathcal{R}},$$

where $\mathcal{R}$ is the gas constant and μ the mean atomic weight per particle (Spruit 2010). Hence, the temperature can be estimated as $\min(T, T_{\rm disc})$, where

$$T \approx \frac{\gamma - 1}{1 - X} \Lambda^{-1} m^{6/7} L_{39}^{2/7} B_{12}^{-4/7} R_6^{-10/7} \left[1 - \frac{\Omega}{\Omega_{\rm K}}\right]^2\ \text{keV},$$

where X is the hydrogen mass fraction. The typical dimensionless thermal velocity of protons $\beta_{\rm th} = v_{\rm th}/c$ at the inner disc radii is

given by

$$\beta_{\rm th} = \frac{1}{c}\left(\frac{3k_{\rm B}T}{m_{\rm p}}\right)^{1/2} \approx 0.056\left(\frac{\gamma-1}{1+X}\right)^{1/2}\Lambda^{-1/2}m^{3/7} \times L_{39}^{1/7}B_{12}^{-2/7}R_6^{-5/7}\left|1-\frac{\Omega}{\Omega_{\rm K}}\right|, \quad (16)$$

We take this velocity as the initial velocity of the accretion flow along the magnetic field lines.

The accretion disc has a certain geometrical thickness, which is defined by hydrostatic balance in the vertical direction (Shakura & Sunyaev 1973) and affected by the origin of opacity (Suleimanov et al. 2007). The disc can be divided into three zones according to the dominating pressure and opacity sources. Gas pressure and Kramer opacity dominate in the outer regions of the accretion disc (C-zone). The relevant disc scaleheight is given by

$$\left(\frac{H}{r}\right)_{\rm C} = 0.056\,\alpha^{-1/10}L_{39}^{3/20}m^{-21/40}R_6^{3/20}r_8^{1/8}, \quad (17)$$

where $r_8 = r/10^8$ cm is the dimensionless radial coordinate. Gas pressure and electron scattering dominate in the intermediate zone (B-zone), where

$$\left(\frac{H}{r}\right)_{\rm B} = 0064\,\alpha^{-1/10}L_{39}^{1/5}m^{-11/20}R_6^{1/5}r_8^{1/20}, \quad (18)$$

and radiation pressure may dominate in the inner zone (A-zone), where

$$\left(\frac{H}{r}\right)_{\rm A} = 0.1\frac{L_{39}R_6}{m}r_8^{-1}. \quad (19)$$

The boundary between B- and C-zones is at $r_{\rm BC} \approx 9\times10^8\,L_{39}^{2/3}m^{-1/3}R_6^{2/3}$ cm, while the boundary between A- and B-zones is at $r_{\rm AB} \approx 2.2\times10^8\,L_{39}^{16/21}m^{-3/7}R_6^{16/21}$ cm.

At mass accretion rates above *few* $\times\,10^{18}$ g s^{-1} (see equation 5), the disc is interrupted at the radiation dominated A-zone. According to equation (19), geometrical thickness can be comparable to the magnetospheric radius at $L \gtrsim 6\times10^{39}\,\Lambda^{7/9}B_{12}^{4/9}m^{8/9}R_6^{1/3}$ (Lipunov 1982; Mushtukov et al. 2015a), but increase of accretion disc thickness can be stopped if accretion disc becomes advection-dominated (Lasota et al. 2016). Hence, the geometrical thickness of accretion disc given by equation (19) can be overestimated.

The geometrical thickness gives the initial coordinate λ from which the accretion flow starts its motion along magnetic field lines. We assume that the accretion flow starts with typical thermal velocity defined by interaction between the accretion disc and the magnetosphere at $R_{\rm m}$ (equation 16). It might be important for the case of extremely high-mass accretion rates, when the disc is interrupted at its radiation dominated zone (A-zone) and geometrically thick there.

4 NUMERICAL RESULTS

We solve equation (7) numerically for a given NS mass, spin period and surface magnetic field strength, taking the initial velocity to be equal to the thermal velocity of protons at the inner radius of accretion disc (equation 16). The initial coordinate is defined by the geometrical thickness of accretion disc $\lambda_{\rm ini} = {\rm atan}(0.5H/R)$ at the magnetospheric radius.

The typical velocity profiles and corresponding optical thickness distributions over the magnetospheric surface are given by

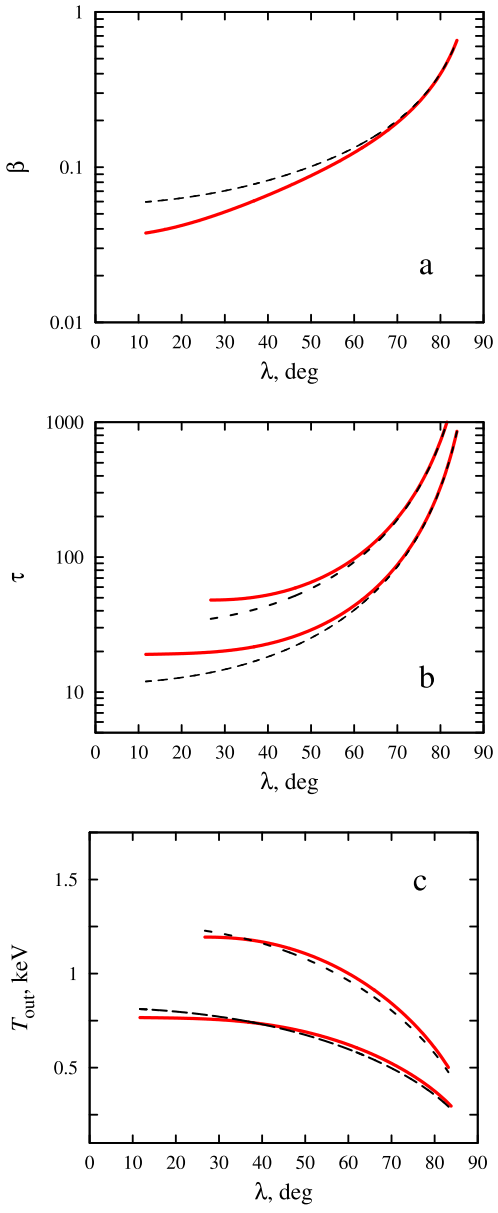

Figure 2. The dimensionless velocity (a), optical thickness (b) and effective outer temperature (c) at the dipole surface of the accreting NS as a function of coordinate λ. Red solid and dashed black lines are given for NS spinning with period $P = 1$ s and non-rotating NS, respectively. The accretion flow velocity is not affected significantly by the mass accretion rate and the curves at (a) correspond to accretion luminosity 5×10^{39} erg s^{-1}. Two sets of curves on (b) and (c) plots are given for accretion luminosity of 5×10^{39} erg s^{-1} *(lower)* and 10^{40} erg s^{-1} *(upper)*. Magnetic field strength is $B = 10^{13}$ G. The parameters used in the calculations: $M = 1.4\,{\rm M}_\odot$, $R = 10^6$ cm, $\Lambda = 0.5$.

Fig. 2a,b. The mass accretion rate and optical thickness define the surface temperature $T_{\rm out}$ (see Fig. 2c). The rotation of NS affects the surface temperature only slightly. According to numerical solutions of equation (7), the typical time-scale of motion of material between the magnetospheric radius and NS surface is $\sim(0.1\div1)$ s. The accretion flow receives the major part of final kinetic energy in the very vicinity of an NS, where the influence of radiation and centrifugal forces is negligible. As a result, the final velocity of matter near NS surface is affected by mass accretion rate only slightly and

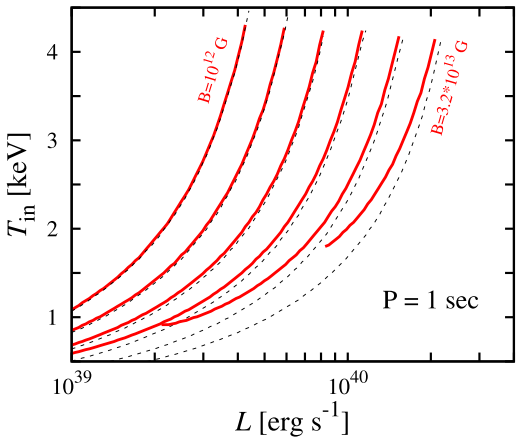

Figure 3. The internal temperature T_{in} as a function of accretion luminosity is shown by red solid lines for NS spinning with period $P = 1$ s and by black dashed lines for non-rotating NS. Different curves correspond to different magnetic field strength: $10^{12}, 2 \times 10^{12}, 4 \times 10^{12}, 8 \times 10^{12}, 1.6 \times 10^{13}, 3.2 \times 10^{13}$ G (from left to right). The upper ends of red curves are defined by condition of super-critical disc at the magnetospheric radius (defined by the disc scale height becoming comparable to the magnetospheric radius). The parameters used in the calculations: $M = 1.4\,M_\odot$, $R = 10^6$ cm, $\Lambda = 0.5$.

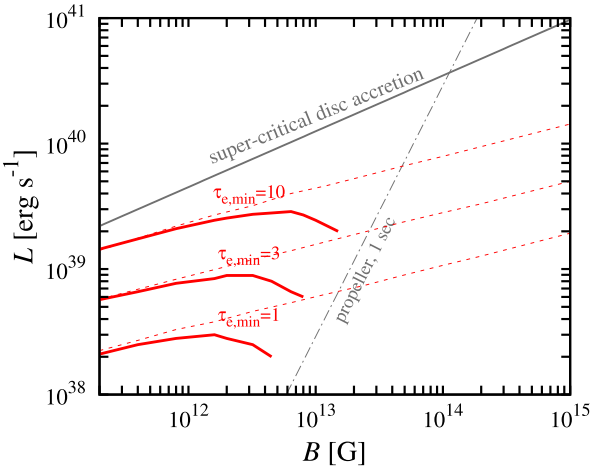

Figure 4. The accretion luminosities where the minimal optical thickness of the envelope due to electron scattering is equal 1, 3 and 10 are given by red solid lines (spin period of NS is taken to be $P = 1$ s) and red dashed lines (non-rotating NS). The grey dashed-dotted line shows the limiting luminosity due to the propeller effect for spin period $P = 1$ s. The centrifugal force becomes essential when the accreting NS is close to the limiting propeller luminosity: the force slows down the accretion flow and makes it optically thicker. The grey solid line limits the region of super-critical disc accretion given by (6). The parameters used in the calculations: $M = 1.4\,M_\odot$, $R = 10^6$ cm, $\Lambda = 0.5$.

earlier theoretical constructions on the structure of X-ray flux forming region (Basko & Sunyaev 1976b; Mushtukov et al. 2015b,a,c) are not influenced by dynamics in the accretion curtain.

The internal temperature T_{in} depends on the mass accretion luminosity and magnetic field strength (see Fig. 3). The temperature is affected by the spin period of the NS because rotation influences the velocity (and therefore the local optical thickness) of accretion flow due to the centrifugal force.

Because of the geometry of the accretion flow, the optical thickness can be high enough to cause advection of photons. The advection process becomes important when the time of photon diffusion (equation 8) becomes comparable to the time over which the material passes a distance equal to the local geometrical thickness of the envelope: $t^\star(\lambda) = d(\lambda)/(c\beta(\lambda))$. It happens at $\cos\lambda \lesssim 4\cos\lambda_0 L_{39}^{2/7} B_{12}^{2/21}$. Therefore, the advective zone is located very close to the NS surface even at accretion luminosity $L \sim 10^{39} \div 10^{40}$ erg s^{-1}. We do not take advection in the accretion envelope into account.

The matter velocity of the accretion flow is significantly smaller than free-fall velocity all over the envelope except the regions close to NS surface. As a result, the estimation of optical thickness from the assumption of free-fall velocity is underestimated and the accretion curtain becomes optically thick already at $L \gtrsim 10^{39}$ erg s^{-1} (see Fig. 4). Therefore, ULXs powered by accretion on to magnetized NS have to be surrounded by the optically thick envelope. The minimal optical thickness on the magnetosphere is affected significantly by centrifugal force if the accretion luminosity becomes comparable to the limiting propeller luminosity: the centrifugal force reduces the velocity along magnetic field lines, which leads to increasing of optical thickness.

5 SUMMARY

The accretion on to magnetized NS goes through the accretion curtain at the magnetosphere. In the case of extremely high-mass accretion rates typical for ULXs, the accretion curtain becomes closed and optically thick (see Fig. 4). This affects the dynamics of matter in the curtain and the basic observational manifestation of the accreting NS at luminosity above $few \times 10^{39}$ erg s^{-1}.

The closed accretion curtain intercepts and reprocesses the initially hard radiation from the central object into blackbody like radiation of temperature that depends on the local optical thickness and total accretion luminosity (see Fig. 2c). Hence, the accretion curtain manifests itself by multi-colour blackbody spectrum, which varies with the viewing angle and can be dominated by the curtain temperature. In this case, the total spectrum can be fitted by double blackbody, where the harder component corresponds to accretion envelope and low-energy component corresponds to an advection dominated accretion disc. Variations of viewing angle due to NS spin lead to variations of the observed spectrum and cause observed pulsations. Because the accretion disc provides a non-pulsating low-energy component in the spectrum, the pulsed fraction is expected to be higher in the higher energy band. These statements are in agreement with observational data: the spectrum of pulsating ULX-1 in NGC 5907 is well-described by multi-colour blackbody (Fürst et al. 2017), while the pulsed fraction is, indeed, higher in the higher energy band. It is interesting, that the spectra of several ULXs are well fitted with a double blackbody model (Stobbart, Roberts & Wilms 2006; Kajava & Rico-Villas 2016).

At larger time-scales the viewing angle can also vary due to precession of the magnetic dipole (Lipunov & Shakura 1980) giving rise to super-orbital variability. The precession period of the NS can be roughly estimated:

$$t_{pr} \approx 1.5 \times 10^4 \frac{\mu_{30}^{-2} I_{45} R_{m,8}^3 P^{-1}}{\cos\psi(3\cos\zeta - 1)} \text{ years}, \quad (20)$$

where ψ is the angle between the normal to the accretion disc plane and NS spin axis, ζ is the angle between the spin axis and magnetic field axis, $\mu_{30} = B_{12} R_6^3$ is NS magnetic moment and I_{45} is NS moment of inertia. If NS has surface dipole magnetic field $>10^{14}$ G, the precession period can be about a year. It is interesting

that a few ULXs including bright pulsating ULX-1 in galaxy NGC 5907 (Israel 2016b) show modulation of a photon flux with typical period of a few months: pulsating M82 X-2 – 55 d (Kong et al. 2016), M82 X-1 – 62 d (Kaaret, Simet & Lang 2006), pulsating ULX NGC 7793 P13 – 65 d and 3000 d (Hu et al. 2017), pulsating ULX-1 NGC 5907 – 78 d (Walton et al. 2016), NGC 5408 X-1 – 115 d and 243 d (Strohmayer 2009; Han et al. 2012), HLX ESO 243-39 – 375 d (Servillat et al. 2011).

Finally, we conclude the following:

(i) Optically thick accretion envelope affects the observed spectra of ULXs because of reprocessing of X-ray radiation from the central object. In the case of a closed accretion curtain, the spectrum is described by a multi-colour blackbody, which can vary with viewing angle. It is likely that the multi-colour blackbody spectrum of the accretion envelope is dominated by the curtain temperature.

(ii) Optically thick envelope makes cyclotron lines originating from the central object undetectable.

(iii) The curtain affects the observed pulse profile. The observer sees photons that have been reprocessed by the envelope and re-emitted from a much more extended photosphere of a geometrical size comparable to the geometrical size of NS magnetosphere. This explains a difference between typical pulse profiles of XRPs and pulsating ULXs: in case of normal XRPs, observer detects photons from the central object and the pulse profile is disturbed by the accretion curtain, while in the case of ULXs, the pulse profile is totally defined by emission from the envelope.

(iv) In the case of normal XRPs, velocity of the matter in the accretion curtain is almost unaffected by radiation pressure. In the case of ULXs powered by accretion on to a NS, the velocity of material on the magnetosphere is different, but the velocity near the NS surface is still close to free-fall velocity. As a result, the developed theoretical models of the geometry of illuminating regions are valid (Basko & Sunyaev 1976b; Mushtukov et al. 2015a).

ACKNOWLEDGEMENTS

This research was supported by the Russian Science Foundation grant 14-12-01287 (AAM) and the German research Foundation (DFG) grant WE 1312/48-1 (VFS). Partial support comes from the EU COST Action MP1304 ‘NewCompStar’.

REFERENCES

Bachetti M. et al., 2014, Nature, 514, 202
Balbus S. A., Hawley J. F., 1991, ApJ, 376, 214
Basko M. M., Sunyaev R. A., 1976a, Soviet Astron., 20, 537
Basko M. M., Sunyaev R. A., 1976b, MNRAS, 175, 395
Dall’Osso S., Perna R., Stella L., 2015, MNRAS, 449, 2144
Doroshenko V., Santangelo A., Ducci L., 2015, A&A, 579, A22
Ekşi K. Y., Andaç İ. C., Çıkıntoğlu S., Gençali A. A., Güngör C., Öztekin F., 2015, MNRAS, 448, L40
Frank J., King A., Raine D. J., 2002, Accretion Power in Astrophysics, 3rd edn. Cambridge Univ. Press, Cambridge
Fürst F., 2017, ApJ, 834, 77
Fürst F. et al., 2016, ApJ, 831, L14
Han X., An T., Wang J.-Y., Lin J.-M., Xie M.-J., Xu H.-G., Hong X.-Y., Frey S., 2012, Res. Astron. Astrophys., 12, 1597
Harding A. K., Lai D., 2006, Rep. Prog. Phys., 69, 2631
Hu C.-P., Li K. L., Kong A. K. H., Ng C.-Y., Chun-Che Lin L., 2017, ApJ, 835, 9
Illarionov A. F., Syunyaev R. A., 1972, Soviet Astron., 16, 45
Ingram A. R., 2016, Astron. Nachr., 337, 385
Israel G. L. et al., 2016, preprint (arXiv:1609.07375)
Israel G. L. et al., 2017, MNRAS, 466, L48
Ivanov V. V., 1969, Radiative Transfer and Spectra of Celestial Bodies Nauka, Moscow
Kaaret P., Simet M. G., Lang C. C., 2006, ApJ, 646, 174
Kajava J. J. E., Rico-Villas F., 2016, preprint (arXiv:1609.03941)
King A., Lasota J.-P., 2016, MNRAS, 458, L10
Kong A. K. H., Hu C.-P., Lin L. C.-C., Li K. L., Jin R., Liu C. Y., Yen D. C.-C., 2016, MNRAS, 461, 4395
Lai D., 2014, EPJ Web Conf., 64, 1001
Lasota J.-P., Vieira R. S. S., Sadowski A., Narayan R., Abramowicz M. A., 2016, A&A, 587, A13
Lipunov V. M., 1982, Soviet Astron., 26, 54
Lipunov V. M., Shakura N. I., 1980, Soviet Astron. Lett., 6, 28
Lyubarskii Y. E., 1997, MNRAS, 292, 679
Mushtukov A. A., Nagirner D. I., Poutanen J., 2012, Phys. Rev. D, 85, 103002
Mushtukov A. A., Suleimanov V. F., Tsygankov S. S., Poutanen J., 2015a, MNRAS, 454, 2539
Mushtukov A. A., Suleimanov V. F., Tsygankov S. S., Poutanen J., 2015b, MNRAS, 447, 1847
Mushtukov A. A., Tsygankov S. S., Serber A. V., Suleimanov V. F., Poutanen J., 2015c, MNRAS, 454, 2714
Mushtukov A. A., Nagirner D. I., Poutanen J., 2016, Phys. Rev. D, 93, 105003
Parfrey K., Spitkovsky A., Beloborodov A. M., 2016, ApJ, 822, 33
Poutanen J., Mushtukov A. A., Suleimanov V. F., Tsygankov S. S., Nagirner D. I., Doroshenko V., Lutovinov A. A., 2013, ApJ, 777, 115
Revnivtsev M., Churazov E., Postnov K., Tsygankov S., 2009, A&A, 507, 1211
Servillat M., Farrell S. A., Lin D., Godet O., Barret D., Webb N. A., 2011, ApJ, 743, 6
Shakura N. I., Sunyaev R. A., 1973, A&A, 24, 337
Shtykovskiy P., Gilfanov M., 2005, A&A, 431, 597
Siuniaev R. A., Shakura N. I., 1977, Pisma v Astron. Zh., 3, 262
Spruit H. C., 2010, preprint (arXiv:1005.5279)
Stobbart A.-M., Roberts T. P., Wilms J., 2006, MNRAS, 368, 397
Strohmayer T. E., 2009, ApJ, 706, L210
Suleimanov V. F., Lipunova G. V., Shakura N. I., 2007, Astron. Rep., 51, 549
Syunyaev R. A., 1976, Soviet Astron. Lett., 2, 111
Tsygankov S. S., Lutovinov A. A., Doroshenko V., Mushtukov A. A., Suleimanov V., Poutanen J., 2016a, A&A, 593, A16
Tsygankov S. S., Mushtukov A. A., Suleimanov V. F., Poutanen J., 2016b, MNRAS, 457, 1101
Walter R., Lutovinov A. A., Bozzo E., Tsygankov S. S., 2015, A&A Rev., 23, 2
Walton D. J. et al., 2016, ApJ, 827, L13

This paper has been typeset from a TEX/LATEX file prepared by the author.